Understanding the transport enhancement of poly (vinyl alcohol) based hybrid membranes with dispersed nanochannels for pervaporation application

Yang, G, Xie, Zongli, Doherty, Cara M, Cran, Marlene, Ng, D and Gray, Stephen (2020) Understanding the transport enhancement of poly (vinyl alcohol) based hybrid membranes with dispersed nanochannels for pervaporation application. Journal of Membrane Science, 603. ISSN 0376-7388

Understanding the transport enhancement of poly (vinyl alcohol) based hybrid membranes with dispersed nanochannels for pervaporation application

Guang Yang[a,b], Zongli Xie[b,*], Cara M. Doherty[b], Marlene Cran[a], Derrick Ng[b], Stephen Gray[a,*]

[a] *Institute for Sustainable Industries and Liveable Cities, Victoria University, PO Box 14428, Melbourne, Vic. 8001, Australia.*

[b] *CSIRO Manufacturing, Private Bag 10, Clayton South, Vic. 3169, Australia.*

Corresponding authors:

** Email：stephen.gray@vu.edu.au; Tel. +61-3-9919-8097*

** Email: zongli.xie@csiro.au; Tel. +61-3-9545-2938*

Abstract

Hybrid membranes, featuring combinations of inorganic and organic materials at the nanometre or molecular level, have been widely reported as providing superior separation performance compared with the traditional polymeric membranes. However, for rational design of membranes, there remains a major doubt as to how each constituent functions in the separation process. Herein, carbon nanotube (CNT) incorporated poly (vinyl alcohol) (PVA) membranes were analysed using pervaporation (PV) process for aqueous mixture separation. The impacts of CNT on the functional properties, morphologies and microscale structures of the PVA/CNT hybrid membranes was investigated by ATR-FTIR, AFM, SEM and positron annihilation lifetime spectroscopy (PALS). Further, a comparison of the interactions between the membrane and solvents (water and ethanol) were identified by swelling test and XRD. The resultant PVA/CNT hybrid membranes were then subject to both desalination and dehydration of ethanol. The results showed that PVA exhibited preferential adsorption of water over ethanol. The addition of CNT enlarged the fractional free volume (FFV) and enhanced water diffusivity

(up to 185%), which indicated a diffusion-dominated type of the PVA/CNT hybrid membranes with a synergistic effect of CNT on water transport. The transport of Na^+ ions through the membrane was examined to be with larger activation energy than that of ethanol during the separation process. This work investigated the state of polymer as well as the effect of nanofillers in the separation of water vs. non-volatile or volatile component for the first time, which can provide in-depth understanding of the polymer-based hybrid membranes for practical applications.

Keywords: Pervaporation; carbon nanotube; poly vinyl alcohol; desalination; dehydration of ethanol.

1. Introduction

Pervaporation (PV) is a membrane process in which the solutes transport through a semi-permeable barrier via a route of preferential adsorption, permeation and desorption as described by the generally accepted solution-diffusion theory [1-3]. Unlike conventional pressure-driven membrane processes such as microfiltration (MF) [4], ultrafiltration (UF) [5], nanofiltration (NF) [6] and reverse osmosis (RO) [7], PV involves a flow of gas or vacuum at the downstream side of the membrane, which causes a partial pressure difference for continuous separation. A phase change from liquid to vapor is observed across the membrane [8], with the membrane being active in determining selectivity [9]. As such, PV shows notable advantages in separating similar-boiling point and azeotropic mixtures over commonly utilized distillation [10]. Depending on the physicochemical properties, the PV membranes can exhibit hydrophilic or organophilic (hydrophobic) property. The applications of PV include dehydration of solvents, desalination and isolation of organics from aqueous-organic mixtures or anhydrous organic mixtures. The past several decades have witnessed the rapid development of PV in industry, particularly in the application of solvent dehydration using hydrophilic membranes. The

first industrial alcohol-water separation apparatus was establish by GFT (Germany) in 1984 [9]. From then on, large-scale applications have been developed rapidly by companies including PolyAn GmbH (Germany), Pervatech B.V. (Netherlands), DeltaMem AG (management buy-out of Sulzer, Switzerland) and Mitsubishi (Japan).

Although module construction and process optimization are indispensable for the development of PV, separation ultimately relies on the membrane materials as they determine the mass transfer characteristics [11]. So far, polymeric [12], inorganic [13] and hybrid materials [14] have been extensively developed in attempts to advance the PV process. Hybrid membranes in particular are the most appealing in pursuing high selectivity, permeability, processability and long term stability. [1]. With the inherited superior merits from both polymeric and inorganic membranes, hybrid membranes are usually obtained by integrating the polymer matrix with inorganic fillers via physical blending [15], sol-gel method [16], or layer by layer self-assembly [17], and are proven to address the inherent issues of polymeric membranes (swelling, poor chemical and thermal stability) and inorganic membranes (inferior film formation, highly brittle and unavoidable defects) [18-21]. Featuring multiphase (typically polymer phase, inorganic phase and intermediate phase) and various interactions (van der Waals force, hydrogen bond, π-π interaction, covalent and ionic bonds) spanning from nanoscale to macroscale, the integration of these two disparate building blocks enables high flexibility toward rational structure design of membrane, thus exhibiting new opportunities capable of tackling the trade-off effect of higher flux at the expense of reduced selectivity [22]. For hydrophilic PV, poly (vinyl alcohol) (PVA) is well suited as a membrane material due to its high affinity to water and excellent film-forming properties. However, swelling and possible dissolution in aqueous environment hinders its practical application [23, 24]. Modification of PVA by either chemical crosslinking or blending with

nanofillers is a prerequisite before use. PVA is often crosslinked with glutaraldehyde, maleic acid and so forth because hydroxyl groups are reactive with aldehydes or carboxylic acid groups [25]. Although crosslinking restrains swelling and ensures the stability of the membrane, it usually causes the reduction of hydrophilic groups (the hydrophilicity of the membrane) and impedes the molecule transport [26, 27]. Comparatively, PVA based organic-inorganic hybrids provide a judicious strategy to further enhance the performance as they can possess the effective cross-linking between PVA chains with crosslinkers while with the loaded nanofillers exhibiting specific functions.

To date, zeolite, silica (SiO_2), titanium dioxide (TiO_2), carbon nanotube (CNT), graphene oxide (GO), graphene oxide quantum dot (GOQD) and metal-organic framework (MOF) have been successfully incorporated into the PVA matrix with enhanced separation performance [28-33]. Based on the morphology and geometry, they can be classified into two types: permeable nanofillers and impermeable nanofillers as shown in Fig. 1. For nanoparticles (e.g., SiO_2, TiO_2 and GO) incorporated membranes, the dispersed phase is not permeable to the solutes (Fig. 1a) which results in a long and tortuous path through the polymer continuous phase or the polymer-filler interface. On the other hand, the dispersed porous fillers such as MOF and CNT, can provide an additional permeating pathway (Fig. 1b). In that case, transport through the dispersed phase can be usually described as molecular sieving, surface adsorption, or bulk diffusion [34-36]. Similar to aquaporins with biological channels for fast water transport in the biological-cell membranes, CNT as permeable nanofiller has similar structure comprised of cylindrical carbon [37]. The spiralling of graphite sheets provides a smooth, narrow and hydrophobic nanochannel for mass transport and it is reported that structure facilitates the formation of confined water chains, as well as bearing weak interactions with water molecules for nearly barrier-free transport [38]. Previous studies have reported remarkable enhancements in the water permeation

flux of the CNT incorporated membranes such as polyethersulfone (PES) , polyamide (PA) and polyvinylidene fluoride (PVDF) [37, 39, 40]. Moreover, CNT has molecular sieving effect depending on the diameter of the inner pore. A 0.93 nm diameter CNT or functionalized 1.09 nm diameter CNT showed a salt rejection of over 95% [41]. However, for CNT incorporated membranes, even though the diameter of CNT is much larger than the solutes, high separation performance of the membrane can still be obtained. For example, Lee et al. [37] showed that the CNT of 10-20 nm diameter in polyamide matrix exhibited a higher water flux than PA without CNT while there was almost no sacrifice of salt rejection. Our previous study also demonstrated significant increases in permeation flux of the crosslinked PVA/CNT hybrid membranes with high rejection for sodium chloride (NaCl) [32]. However, nanoscale physicochemical changes of the polymer matrix such as free volume and crystallinity which are highly associated with the permselectivity of the membrane, have been rarely studied for hybrid membranes. Although CNT incorporated PVA membranes have been researched in PV process [24, 42-44], the CNTs used were usually derived from acid oxidation under heating. That made the influence of the CNT functional groups unclear due to the complex composition (-OH, -COOH and -C=O) [45, 46]. The PVA matrix has variable types (crosslinked or uncrosslinked), which calls for comparison to guide rational membrane design. More importantly, it is worthwhile investigating the comprehensive separation capability of PVA based membranes toward both desalination and alcohol dehydration for practical application.

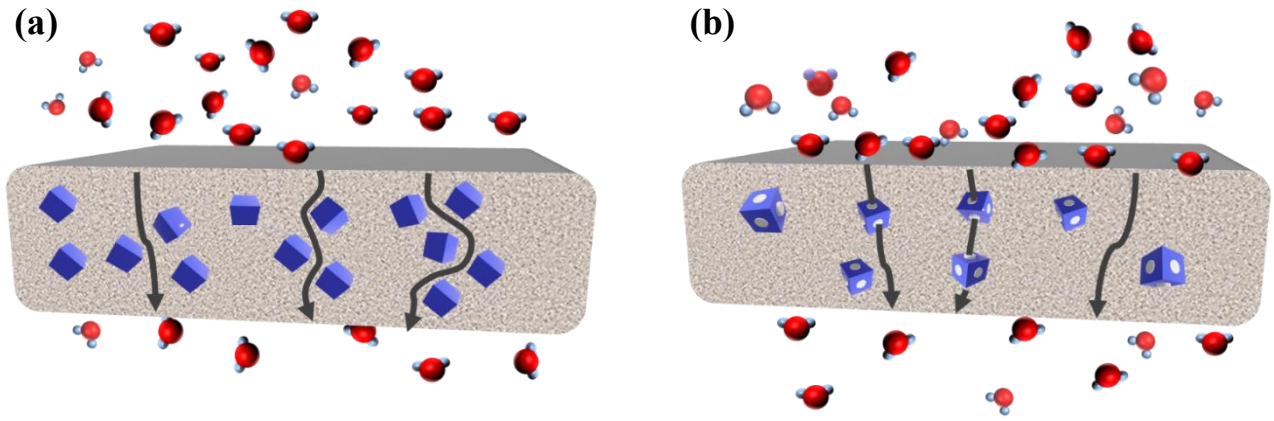

Fig. 1. Permeation through (a) hybrid membrane with impermeable nanofillers and (b) hybrid membrane with permeable nanofillers.

Herein, to address the abovementioned queries and gain further understanding, the transport properties of the PVA/CNT hybrid membranes for both desalination and alcohol dehydration processes were systematically investigated as a necessary extension for its proven separation capability with a particular focus on the effect of various CNT (carboxyl functionalized or nonfunctionalized) on the nano-physicochemical properties of polymer phase. Carboxyl functionalized and pristine CNTs are served as nanofillers to compare the effect of functional groups. Crosslinked and uncrosslinked PVA were employed as the polymer matrixes. As diffusion through the membrane is highly related to the free volume and selective separation to the free volume cavity size, positron annihilation lifetime spectroscopy (PALS) analysis was applied to the PVA based hybrid membranes. In addition, for aqueous mixture separation, PV is subjected to strong interactions between water molecules and hydrophilic membrane materials, and the properties of polymeric membranes in wet condition are usually different compared with those in the dry state. Therefore, detailed wet state polymer phase characterizations (XRD, wet state PALS and swelling) were investigated. This study aims to elucidate how the polymer and nanofillers in hybrid membranes function in separating different type of aqueous

134 mixtures, and to correlate the inherent transport properties of the membrane with PV performance.

135 **2. Experimental**

136 *2.1. Materials*

137 PVA of 98-99% hydrolysed (molecular weight of 160,000 g/mol), maleic acid (MA), *p*-toluene
138 sulfonic acid (98.5% monohydrate), ethanol and NaCl obtained from Sigma-Aldrich were used as
139 received for the experiment. Two kinds of carbon nanotubes, i.e. multiwalled carbon nanotube
140 (MWCNT) as well as functionalised multiwalled carbon nanotube (F-MWCNT) with 3.86 wt% of
141 carboxyl groups were purchased from XFNANO Co. Ltd. The inner diameter of the above carbon
142 nanotubes was in the range 2-5 nm with the outer diameter < 8 nm and the specific surface area > 200
143 m^2/g. The length of MWCNT and F-MWCNT was in the range of 0.5-2 μm. Milli-Q deionised water
144 (18.1 MΩ cm) was used throughout the study.

145 *2.2. Synthesis of PVA based hybrid membranes*

146 Firstly, 100 mg of MWCNT or F-MWCNT was dispersed in 50 mL of ethanol with ultrasonication
147 in an ice bath for 2 h. A mass of PVA powder (12 g) was dissolved slowly in 200 mL of Milli-Q
148 deionised water at 90°C and stirred for 3 h to obtain a homogeneous solution. After cooling to room
149 temperature, blending of the PVA/CNT mixture was realized by the addition of a predetermined
150 amount of MWCNT/ethanol or F-MWCNT/ethanol dispersion to the PVA solution. The composition
151 of the PVA/CNT membranes is presented in Table 1 and all the mass fractions of CNTs, MA and *p*-
152 toluene sulphonic acid were relative to the PVA. For the crosslinked PVA based membranes, specified
153 amounts of MA and *p*-toluene sulfonic acid (catalyst) were dissolved in the PVA solution or

PVA/FMWCNT mixture under stirring for 2 h. After degassing for 24 h, all the resultant mixtures, i.e., the PVA-MA, PVA-CNT, PVA-FCNT, and PVA-MA-FCNT were cast on a plastic plate using a casting bar of 100 μm. After drying for 24 h, the obtained films were detached from the plate and treated under 140 °C in an oven for 2 h as described elsewhere [32].

Table 1

The composition of the fabricated membranes.

Membranes	MWCNT loading (wt%)	F-MWCNT loading (wt%)	MA loading (wt%)	catalyst (wt%)	Membrane thickness (μm)
PVA-MA	-	-	20	1.5	19.5 ± 1.7
PVA-CNT0.5	0.5	-	-	-	20.7 ± 1.6
PVA-CNT1	1	-	-	-	20.5 ± 2.1
PVA-CNT2	2	-	-	-	19.8 ± 2.3
PVA-FCNT0.5	-	0.5	-	-	19.2 ± 2.7
PVA-FCNT1	-	1	-	-	20.3 ± 1.5
PVA-FCNT2	-	2	-	-	20.1 ± 2.2
PVA-MA-FCNT0.5	-	0.5	20	1.5	21.2 ± 2.4
PVA-MA-FCNT1	-	1	20	1.5	19.9 ± 1.9
PVA-MA-FCNT2	-	2	20	1.5	20.9 ± 1.6

2.3. Characterisation of PVA based hybrid membranes

For the characterisation of the fabricated membranes, 3 samples of each type of membranes (PVA-MA, PVA-CNT, PVA-FCNT and PVA-MA-FCNT) were tested. The surface and cross-section morphologies of the fabricated membrane were observed and photographed by Zeiss Merlin Gemini 2 Field Emission Scanning Electron Microscopy (FESEM) and the TECNAI 12 transmission electron microscope (TEM). The surface roughness was probed by atomic force microscope (AFM) using SPM-9700 (SHIMADZU). The presence of functional groups was detected by attenuated total reflectance-Fourier transform infrared (ATR-FTIR) spectroscopy (Perkin-Elmer Spectrum 2000 FTIR instrument).

A Rigaku SmartLab X-ray Diffractometer, operating in parallel beam mode under CuK radiation (45kV, 200mA), equipped with a HyPix-3000 detector, was employed to obtain the X-ray diffraction (XRD) patterns. For the wet state results, samples were immersed with water or ethanol for 96 h to ensure an equilibrium state. The samples were scanned over the 2θ range 10° to 50° rapidly before the evaporation of ethanol. The resultant degree of crystallinity was calculated according to [47]; where X_c is the degree of crystallinity, I_c (2θ) and I_a (2θ) are the X-ray scattering intensity of crystalline region and amorphous region, respectively.

$$X_c = \frac{\int_{2\theta\neq 0} I_c(2\theta)d(2\theta)}{\int_{2\theta\neq 0} I_a(2\theta)d(2\theta) + \int_{2\theta\neq 0} I_c(2\theta)d(2\theta)} \times 100\% \quad (1.)$$

PALS was applied for the average free volume characterisation of both the dry and wet states according to our previous study [29, 48]. Briefly, the membranes were first annealed at 50 °C overnight. Then, they were cut and piled to 4 mm in a nitrogen atmosphere with a Mylar sealed ^{22}Na positron source fixed in the middle of the sample followed by the measurement of an automated EG & GOrtec fast-fast spectrometer. After the dry state characterisation, the membranes were immersed in 3.5 wt% NaCl solution or ethanol overnight and measured in a sealed sample holder to prevent evaporation. The time resolution of the tests was 240 ps and the LT v9 software was used for analysing the resulted spectra [49]. The average pore radius (R), average volume of the free volume elements (V_F) and the fractional free volume (FFV) were obtained by the following equations assuming the free volume elements were distributed as spherical cavities in the polymer [50];

$$\tau_3 = \frac{1}{2}\left[1 - \frac{R}{R+\triangle R} + \frac{1}{2\pi}\sin\left(\frac{2\pi R}{R+\triangle R}\right)\right]^{-1} \quad (2)$$

$$V_F = \frac{4}{3}R^3 \quad (3)$$

$$\mathrm{FFV} = V_F I_3 \quad (4)$$

τ_3 is the o-Ps lifetime; ΔR of 1.66 Å is the empirical electron layer thickness [29] and I_3 is the intensity of o-Ps.

The swelling properties were tested as follows: (1) pre-dried freestanding membrane samples were soaked in DI water or ethanol at ambient temperature for 96 h to reach absorption equilibrium; (2) the water or ethanol adsorbed on the surface were removed by tissues manually to obtain W_s as the wet weight, and (3) the samples were then placed in an oven at 25 °C for 30 h and measured again for the dry weight of W_d. The degree of swelling (DS) was calculated in Eq (5).

$$s = \frac{w_s - w_d}{w_d} \times 100\% \quad (5)$$

2.4. Pervaporation performance evaluation

PV separation tests were conducted using a bench-scale PV set-up as described elsewhere [14]. To be specific, a membrane with separating area of 12.6 cm^2 was employed. A predetermined NaCl solution or ethanol/water mixture was circulated with a flow rate of 50 mL/min on the upstream side of the membrane by a Masterflex® peristaltic pump. The feed temperature was kept as required via a water bath. 1 Torr of vacuum pressure was maintained on the permeate side by a vacuum pump. Finally, the permeating vapor were condensed in a dry-ice or liquid nitrogen cold trap. The performance tests were performed on 3 samples of each type of membranes (PVA-MA, PVA-CNT, PVA-FCNT and PVA-MA-FCNT) and conducted for 3 h upon reaching a stable state whereas the long-term tests were operated for 30 h. Permeance (the normalized driving force for permeation flux in a unit of GPU = 1

$\times 10^{-6}$ m^3(STP)/m^2 s cmHg), selectivity (α), salt rejection, separation factor (β) for dehydration of ethanol were applied to evaluate the transport properties of the membranes based on Eq (6-10) [51, 52]. Ethanol permeance can also be calculated using Eq (7). The salt concentration of the feed *(C_f)* and permeate (C_p) were derived from a pre-calibrated Oakton® Con 110 conductivity meter. For ethanol dehydration, the ethanol concentration in the permeate side was determined by nuclear magnetic resonance (NMR, Bruker 400 Ultrashield with Icon NMR analysis software).

$$J_i = \frac{M_i}{A \times t} \tag{6}$$

$$(\mathrm{P}/l)_i = \frac{J_i}{P_{i0} - P_i} = \frac{J_i}{\gamma_{i0} x_{i0} P_{i0}^{sat} - P_{il}} \tag{7}$$

$$R = \frac{C_f - C_p}{C_f} \times 100\% \tag{8}$$

$$\alpha = \frac{\left(P/l\right)_i}{\left(P/l\right)_j} \tag{9}$$

$$\beta = \frac{Y_i/Y_j}{X_i/X_j} \tag{10}$$

For PV dehydration of ethanol, the weight fractions of each component *i* and *j* in the feed and permeate were denoted as X and Y, respectively. J_i (kg/m^2 h) represented the permeation flux of component *i* in which M_i (mass of component *i* in the permeate side) was divided by the product of A (the effective membrane area) and *t* (permeation time).

For permeance calculation, J_i was converted to the volume under standard temperature and pressure (STP). P_{i0} and P_{il} represented the partial pressures of *i* in the feed and permeate side,

respectively. γ_{i0} (achieved by ASPEN HYSYS program) and x_{i0} were the activity coefficient and the mole fraction of *i* in the feed solution,respectively. P_{i0}^{sat} was derived from the saturated vapor pressure of pure component *i* whereas the pressure on the permeate side (P_{il}) was negligible. *l* (m) was the thickness of the membrane.

2.5. Penetrant diffusion properties

The water diffusion coefficient D_w (m^2/s) was investigated based on the time lag method [53] using DI water as the feed. In Eq (11), *Q*, *t, l* and C_0 were the total amount of diffusing water per unit surface of the membrane (kg/m^2), time of pervaporation experiment (min), the thickness of the membrane (m) and concentration (kg/m^3) of water in membrane, respectively. The relationship between Q and t, as well as the obtained D are shown in Fig. S4 in the supporting information. NaCl diffusion through the synthetized membranes was investigated by the kinetic desorption method described elsewhere [29]. The diffusivity was determined by Eq (12) where M_t and M_∞ were the amount of NaCl in the solution at time *t* and the total amount when desorption was finished. The solubility, *K,* was the ratio of the equilibrium amount of water or NaCl absorbed into the membrane per unit membrane volume [54]. According to the solution-diffusion model, permeability, *P*, was the product of *D* and *K* (both applicable for water and salt).

$$Q = C_0\left(\frac{D_w t}{l} + \frac{l}{3}\right) \tag{11}$$

$$D_S = \frac{\pi \times l^2}{16}\left[\frac{d\left(\frac{M_t}{M_\infty}\right)}{d\left(\mathrm{t}^{\frac{1}{2}}\right)}\right]^2 \tag{12}$$

$$P = D \times K \tag{13}$$

The relationship between the permeation flux and temperature for pervaporation generally follows the Arrhenius equation (14) where A_i, R, T and E_a were the pre-exponential factor, the gas constant (8.3145×10^{-3} kJ/mol K), the absolute temperature (K) and the apparent activation energy for the permeation (kJ/mol), respectively [55].

$$J_i = A_i exp\left(-\frac{E_a}{RT}\right) \tag{14}$$

3. Results and discussion

3.1. Changes of the fabricated membranes with the addition of CNT.

3.1.1 Functional structure changes of the PVA/CNT hybrid membranes

In Fig. 2a, comparisons between pure PVA, PVA-MA, PVA-CNT1, PVA-FCNT1 and PVA-MA-FCNT1 were performed using ATR-FTIR to identify the bulk chemistry changes that occurred in the PVA/CNT hybrid membranes. In general, the characteristic bands at 3000-3500 cm^{-1}, 2800-3000 cm^{-1}, 1400-1500 cm^{-1} and 1100-1000 cm^{-1}, correspond to the -OH from intermolecular and intramolecular hydrogen bonds, the stretching vibrations of C-H from alkyl groups, $-CH_2$ from PVA backbone and C-OH stretching vibrations, respectively [26]. For the PVA-CNT1 and PVA-FCNT1 samples, the F-MWCNT or MWCNT were physically mixed with PVA (PVA-FCNT spectra comparison with PVA-MA in Fig. S1 in Supporting Information). On the other hand, C=O characteristic bands at a wavenumber of 1710-1750 cm^{-1} and two C-O bands at 1330-1050 cm^{-1} (in the grey area of Fig. 2a.),

which were attributed to the formation of ester groups, were present for PVA-MA and PVA-MA-FCNT1. That implied the -OH from PVA reacted with -COOH from MA or F-MWCNT through dehydration condensation in the presence of catalyst under certain conditions such as the heat treatment. Since the F-MWCNT was functionalized with carboxyl groups, it was possible that they would be esterified with PVA apart from the presence of MA [56]. To further investigate the PVA-MA-FCNT system, Fig. 2b shows the transmittance spectra representing ester groups (grey area) that grew with F-MWCNT loading, indicating that more ester groups were generated upon addition of F-MWCNT. Meanwhile, transmittance in 3000-3500 cm^{-1} region decreased because of the consumption of hydrogen-bonded hydroxyl groups, coinciding with the augment of esterification reactions.

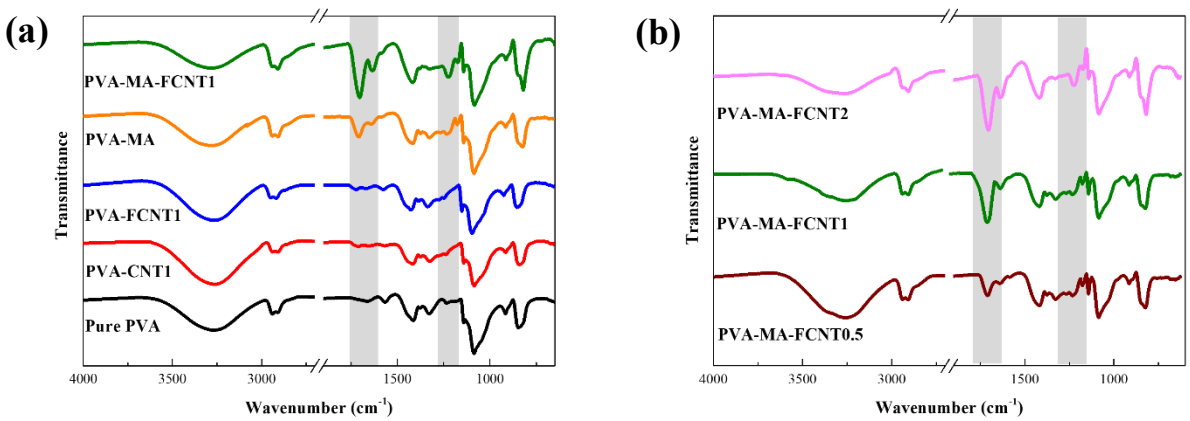

Fig. 2. ATR-FTIR spectra of the PVA based hybrid membranes.

3.1.2 Morphology before and after the addition of CNT

The surface roughness changes of the PVA based hybrid membranes are presented in Fig.3. In comparison with PVA-MA (Ra=69.1 ± 6 nm), the surface roughness of PVA-CNT1 decreased to 25.7 ± 4 nm. The surfaces of the membranes were even smoother with the addition of functionalized CNT, i.e., 10.97 ± 2 nm for PVA-FCNT1 and 12.44 ± 3 nm for PVA-MA-FCNT1. Such surface morphology

transformation can be attributed to the PVA-nanofiller interactions and the subsequent film forming kinetic. Blending of CNT allowed PVA to be less mobile during solvent evaporation and heat-treatment whereas PVA chains without CNT were possible to become highly mobile especially when the heating temperature was higher than its glass transition temperature. Compared with the MWCNT incorporated membrane, the functional groups on F-MWCNT reinforced the interactions with PVA, making it reasonable to exhibit flatter surface. Additionally, the corresponding photographs of the PVA based membranes are shown in Fig. 4. The PVA-MA was transparent whilst the PVA/CNT membranes were dark due to the addition of CNT. According to the photographs, it could be observed that the dispersion of F-MWCNT in PVA was relatively uniform whereas macroscopic domains that were possibly comprised of agglomerated MWCNTs could be found in PVA-CNT1.

The FESEM images of the PVA/CNT hybrid membranes with different CNT loadings are shown in Fig. 5. As can be seen, the surface of the PVA-MA sample (Fig. 5a) was homogeneous without defects such as cracks, ruptures or pinholes. While with the addition of F-MWCNT, the content of inhomogeneous spots which may represent the CNT tips on the surface increased from PVA-MA-FCNT0.5 to PVA-MA-FCNT1 (Fig. 5b to c). Interconnected bundle-like protrusions or wrinkles were observed on the surface of PVA-MA-FCNT2 (Fig. 3d), implying the formation of the CNT agglomeration. The corresponding cross-section pictures of PVA-MA-FCNT1 (Fig. 5e) and PVA-MA-FCNT2 (Fig. 5f) showed good consistency with the surface morphology as the PVA/CNT hybrid materials were distributed across the longitudinal direction. By contrast, for PVA-CNT1 (Fig. 5g), which was with identical CNT loading as PVA-MA-FCNT1, large inclusions resulting from CNT-rich domains or submicroscale entangled bundles became obvious on the membrane surface, suggesting inferior dispersion of MWCNT in PVA compared with that of the F-MWCNT. Besides, the cross-

section of PVA-CNT1 (Fig. 5h) and PVA-CNT2 (Fig. 5i) exhibited increasing agglomeration in the polymer matrix with internal crumpled morphology. It is widely acknowledged that nanomaterials with high surface energy easily agglomerate owing to van der Waals forces [57]. The functionalization of CNT with carboxylic groups changed the hydrophobicity of the outer surface, improving the hydrophilicity and the interfacial interactions with PVA. That is conducive to disentanglement of CNT in the polymer matrix, thus showing good compatibility and uniform dispersion. On the other hand, the increase in the CNT loading induced significant morphological change of PVA-CNT1 and PVA-CNT2, which might result from the development of the entropically-driven phase separation behaviour with the agglomeration of the nanomaterials in the polymer as investigated by Akcora [58].

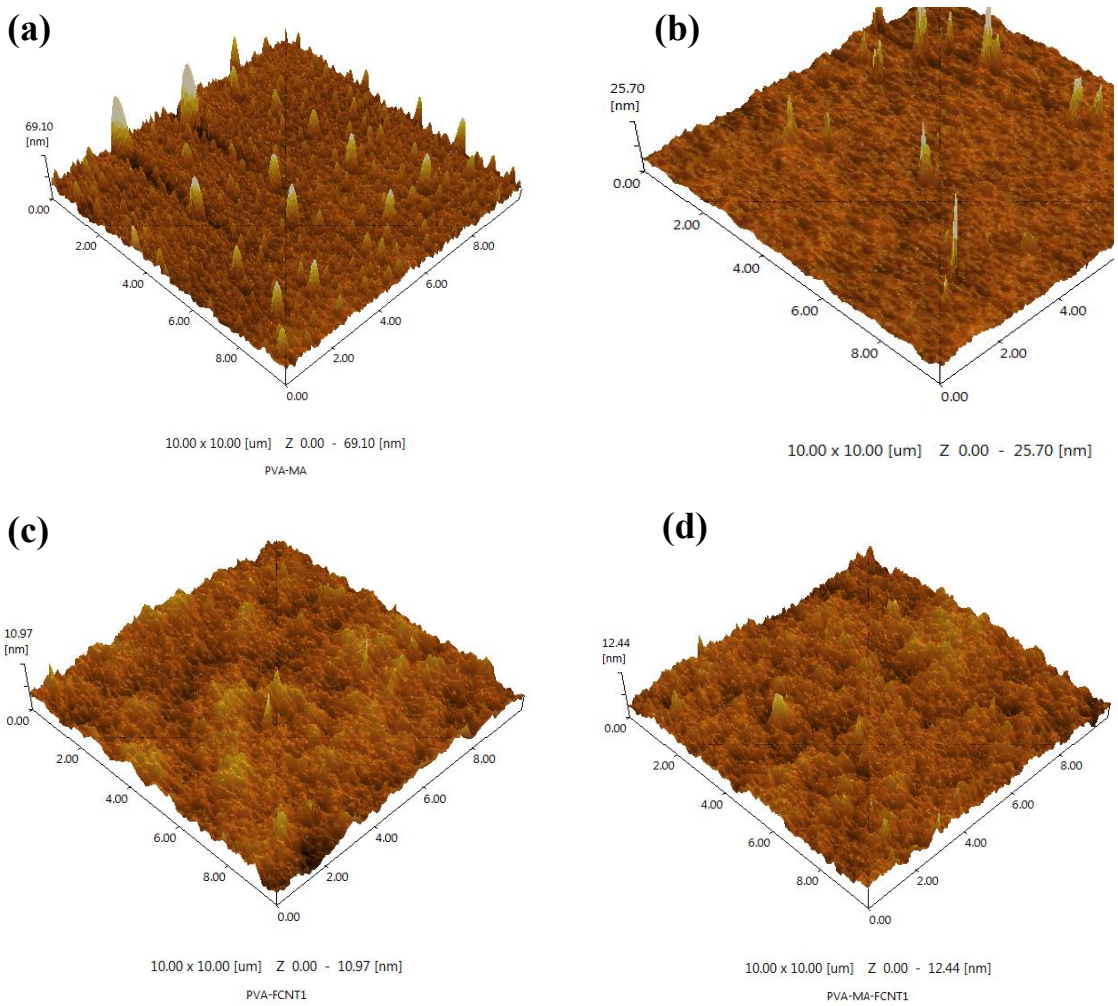

Fig. 3. AFM surface roughness of the PVA based hybrid membranes.

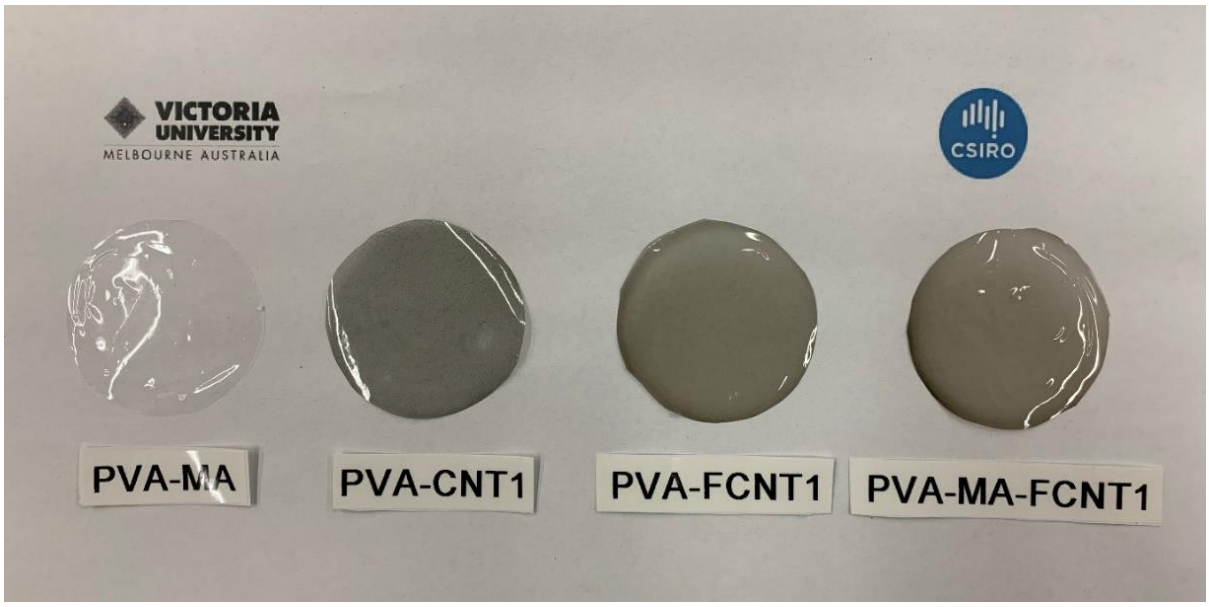

Fig. 4. Optical pictures of the PVA based hybrid membranes.

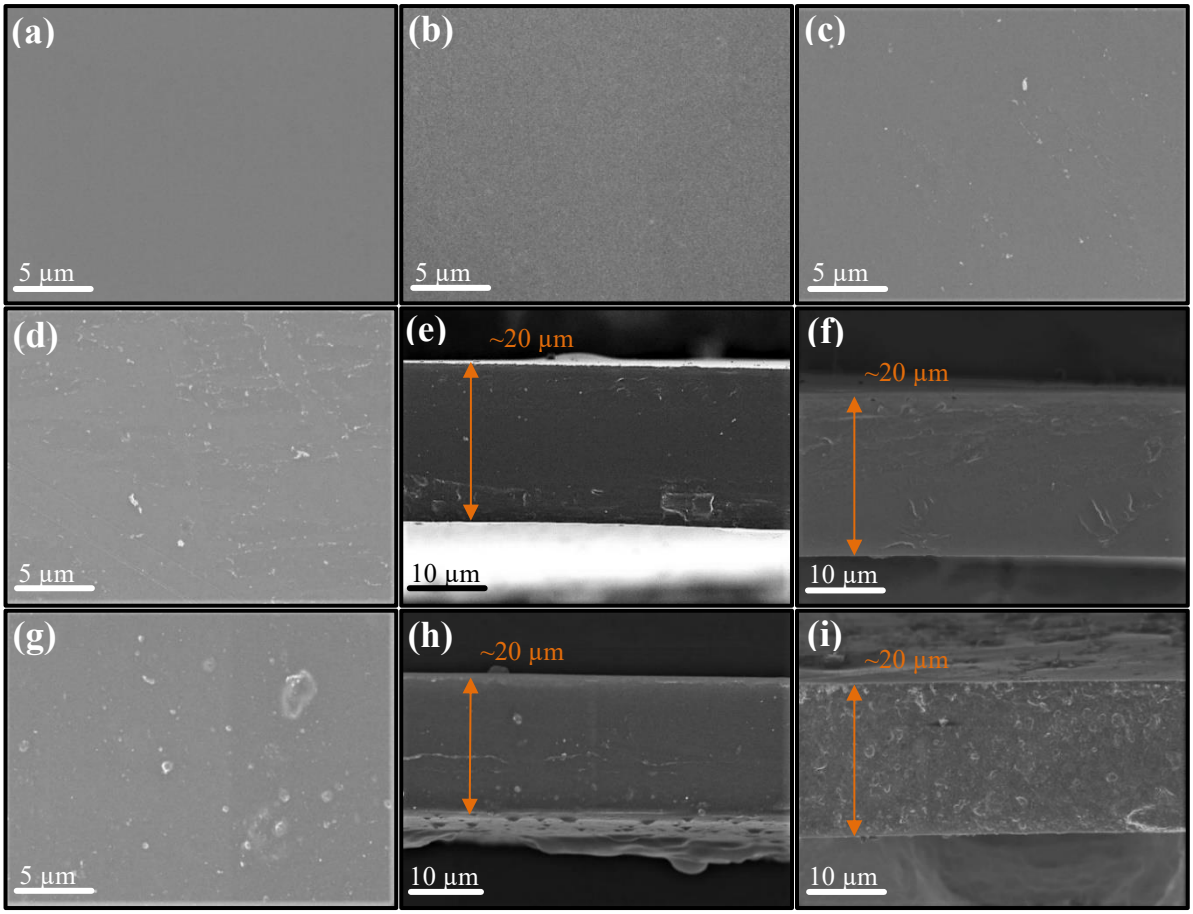

Fig. 5. FESEM surface and cross-section images of (a) surface of PVA-MA; (b) surface of PVA-MA-FCNT0.5; (c) surface of PVA-MA-FCNT1; (d) surface of PVA-MA-FCNT2; (e) cross-section of PVA-MA-FCNT1; (f) cross-section of PVA-MA-FCNT2; (g) surface of PVA-CNT1; (h) cross-section of PVA-CNT1; (i) cross-section of PVA-CNT2. The corresponding thicknesses of the membranes (~ 20 µm) are marked.

369 *3.2. Interactions with water and ethanol*

370 3.2.1 Swelling behaviour in different solvents

371 Table 2 shows the degree of swelling (DS) of the membranes in various solvents at room
372 temperature. Clearly, the DS in water was far greater than that in ethanol for all the membrane samples,
373 showing the solvent-dependent swelling behaviour of the PVA based membranes. It is understandable
374 that chemical crosslinking reduced the number of hydroxyl groups of PVA and that resulted in a
375 decrement of the DS. The DS was further restrained when the F-MWCNT loading for PVA-MA-FCNT
376 was 2 wt%. That was a direct indication of the extra chemical linkage of F-MWCNT and PVA within
377 the membrane. For the blended membranes, swelling in water decreased with the content of CNT,
378 which was mainly attributed to the increased rigidification [56]. The rigidification in turn decreases
379 the mobility of polymer chains as a physical anti-swelling effect. In addition, for the PVA-FCNT
380 membranes, there was strong interaction between the hydrophilic functional groups [59], which further
381 suppressed polymer chain mobility. On the other hand, as PVA is an ethanol-insoluble polymer, the
382 hybrid membranes showed almost complete swelling resistance and it was even further inhibited with
383 CNT content in the polymer for PVA-FCNT and PVA-MA-FCNT membranes. However, it can be
384 observed that the ethanol swelling of PVA-CNT membranes was proportional to MWCNT loading.
385 Due to the hydrophobic nature of MWCNTs, they could be readily dispersed in ethanol and the resulted
386 PVA-CNT membranes were imparted with better compatibility with ethanol, thus showing higher
387 swelling degree compared with others.

388

389

390

Table 2

Degree of swelling for the fabricated membranes in water or ethanol.

Membranes	DS in water（%）	DS in ethanol （%）
PVA-MA	60 ± 5	1.58 ± 5
PVA-CNT0.5	89 ± 6	2.49 ± 0.19
PVA-CNT1	76 ± 5	3.58 ± 0.17
PVA-CNT2	66 ± 5	4.72 ± 0.20
PVA-FCNT0.5	88 ± 7	2.28 ± 0.16
PVA-FCNT1	66 ± 5	1.94 ± 0.15
PVA-FCNT2	50 ± 3	1.59 ± 0.11
PVA-MA-FCNT0.5	60 ± 4	1.37 ± 0.18
PVA-MA-FCNT1	47 ± 3	0.89 ± 0.11
PVA-MA-FCNT2	34 ± 1	0.67 ± 0.09

3.2.2 Effect of solvents on the crystalline properties of the PVA based membranes

Fig. 6 displays the XRD diffraction profiles of both dry and wetted states of the hybrid membranes. For the dry-state membranes in Fig. 6a, strong peaks at 2θ = 19.5 °, referring to the characteristic peaks for the orthorhombic lattice (101) of PVA were present for all the samples which indicated the crystalline region in the semi-crystalline PVA polymer. There was a decrease in this peak intensity for the crosslinked membranes compared with those of the blended membranes. The reason for that was the consumption of hydroxyl groups by the crosslinking reaction. For the samples wetted with ethanol in Fig. 6b, the diffraction profiles were almost identical with those of the dry-state samples except for tiny decreases in the peak intensities. That might be the interference of the trapped ethanol in the polymer matrix. The amorphous portion remained a glassy state in ethanol. However, the XRD patterns of the water-swollen membranes were transformed to two dominant halo-shaped peaks centred around 2θ of 28° and 43°. The diffraction patterns exhibited more of the characteristic peaks of water as reported in previous literature [60]. In that case, there were new intermediate phases including the PVA chains and water molecules, or the CNT and water. It could be demonstrated that a large amount of the

crystalline PVA had been dissolved by long-term contact of water, forming a large swollen amorphous PVA phase. The corresponding degree of crystallinity was calculated as shown in Table 3. Compared with the reduction of crystallinity in ethanol (3.8% for PVA-MA, 7.1% for PVA-CNT1, 4.6% for PVA-FCNT1 and 4.1% for PVA-MA-FCNT1), a significant decrease in PVA crystallinity in water was confirmed with 62.8%, 90.2%, 83.1% and 63.3% for PVA-MA, PVA-CNT1, PVA-FCNT1 and PVA-MA-FCNT1, respectively. Overall, the semi-crystalline nature of dry PVA did not show an obvious difference with ethanol, whereas it was altered by water with significant decrease in the degree of crystallinity as shown by the reduction in crystalline phase [61].

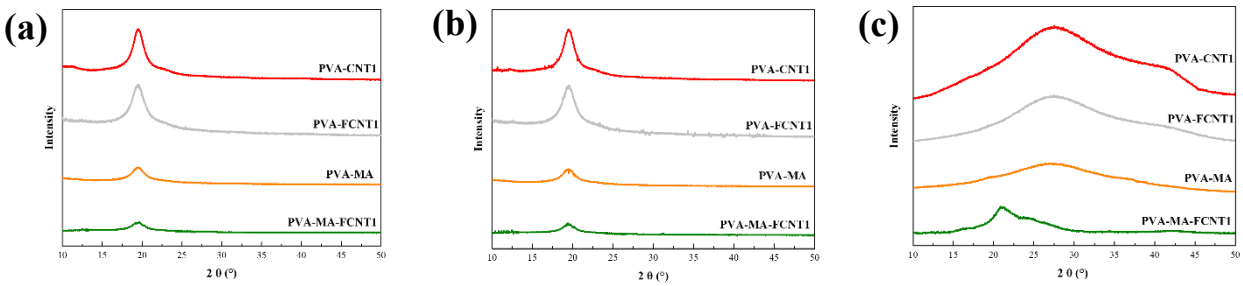

Fig. 6. X-ray diffraction profiles of the membranes in different states; (a) dry state, (b)ethanol wetted state and (3) water wetted state.

Table 3

Degree of crystallinity of the as-fabricated membranes in different environments.

Membranes	Dry	Ethanol	Water
PVA-MA	15.6±3%	15.0±2.2%	5.8±1.1%
PVA-CNT1	36.8±4.1%	36.6±3%	3.6±0.8%
PVA-FCNT1	38.4±2.5%%	37.8±2.7%%	6.5%±0.9%
PVA-MA-FCNT1	9.8±3%	9.4±2.1%	3.6±0.5%

3.2.3 PALS analysis of the PVA based hybrid membranes

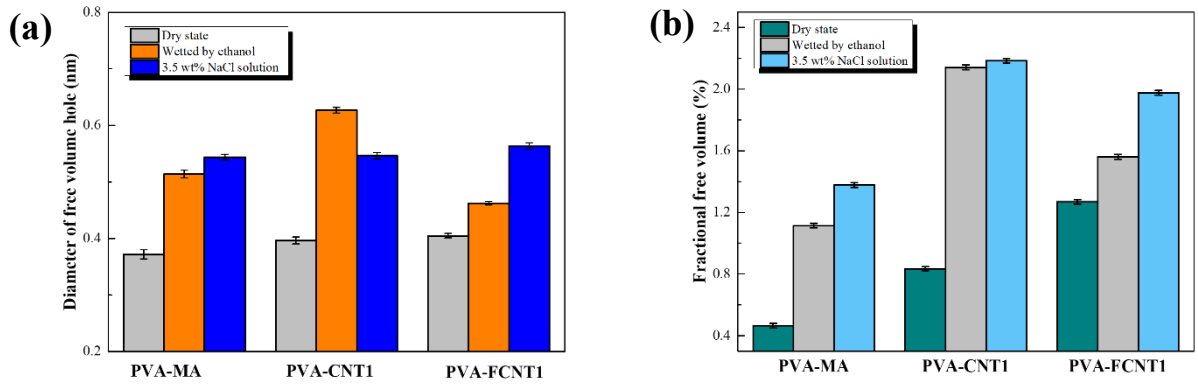

Fig. 7. PALS results of (a) average free volume cavity diameter and (b) FFV.

The changes of the free volume properties for the PVA based hybrid membranes in dry and swollen states were characterized by PALS in terms of free volume cavity diameter (Fig. 7a) and FFV (Fig. 7b). The PVA-MA-FCNT membranes showed signs of positronium inhibition, however, no o-Ps formed which made it difficult for obtaining reliable pore size and intensity data. Therefore, only the PALS results of PVA-MA, PVA-FCNT and PVA-CNT membranes can be discussed in this section. In Fig. 7a, compared with PVA-MA (0.372 ± 0.008 nm), there were notable increases in the diameters for the PVA/CNT hybrid membranes, i.e., 0.396 ± 0.006 nm for PVA-CNT1, 0.405 ± 0.004 nm for PVA-FCNT1. As reported previously [62], a dramatic increase in the interfacial area was usually realized by intercalating nanoscale inorganic fillers of high specific surface area into the polymer matrix, leading to a large amount of volume fraction of interfacial polymer with distinguished properties from the bulk polymer. As a result, the free volume of polymer grew with the addition of nanofillers rather than a compacted structure of the neat polymer. Moreover, the dispersion state of F-MWCNT was much better than MWCNT, resulting in a greater available interface area. That might contribute to a higher free volume diameter for PVA-FCNT1. For the swollen membranes, it could be seen that the diameters were enlarged to 0.514 ± 0.007 nm for PVA-MA, 0.627 ± 0.005 nm for PVA-

452 CNT1, 0.462 ± 0.003 nm for PVA-FCNT1 (ethanol wetted membranes), and 0.544 ± 0.005 nm for
453 PVA-MA, 0.546 ± 0.002 nm for PVA-CNT1, 0.563 ± 0.002 nm for PVA-FCNT1 (water wetted
454 membranes), showing a solvent effect on changing the polymer backbone chain mobility and thus the
455 free volume. However, the hole diameter of PVA-CNT1 in ethanol was significantly different to the
456 others as a result of the affinity and adsorptive property of MWCNT to ethanol.

457 The FFV (Fig. 7b), namely the free volume scaled on the specific volume of the membrane matrix,
458 showed good coherence with the trend of pore size diameters. After the incorporation of carbon
459 nanotube, the FFV of PVA-MA was increased by 79% (PVA-CNT1) and 172% (PVA-FCNT1) for the
460 dry state; 59% (PVA-CNT1) and 43% (PVA-FCNT1) for the water wetted state and 92% (PVA-CNT1)
461 and 40% (PVA-FCNT1) for the ethanol wetted state. It is notable that the FFV of PVA-FCNT1 was
462 much higher than that of PVA-CNT1 in the dry state. That could be reasonably attributed to the better
463 dispersion state of F-MWCNT, effectively disrupting the polymer chain packing. On the other hand,
464 the MWCNT showed good compatibility with ethanol, thus the FFV in ethanol wetted state was
465 obviously higher than that of PVA-FCNT, in line with the pore diameter results. As the diffusion
466 through the membrane is intrinsically related to the microstructure of the membrane, the enrichment
467 of free volume would exert an influence on the transport property and separation performance based
468 on the free volume theory [62].

469 *3.3. PVA/CNT membrane separation performance*

470 3.3.1. Comparison between PV desalination and dehydration of ethanol

471 The PV performance of the synthesized membranes for both desalination and dehydration of
472 ethanol at a feed temperature of 30 °C was evaluated in terms of water permeance, salt rejection and
473 separation factor as depicted in Fig. 8. For desalination (Fig. 8a), the crosslinked PVA network (PVA-

MA) showed salt rejection of 96.5% with water permeance of 6.13×10^4 GPU. After the incorporation of CNT, a significant improvement of the water permeance could be observed. For PVA-CNT1, the water permeance was increased by 116% with respect to that of PVA-MA but a decreased salt rejection of 93.4%. The lower salt rejection of PVA-CNT can be attributed to the severe swelling and inferior dispersion state of MWCNT that increased the nonselective transport (discussion of salt permeability in 3.3.2). The PVA-FCNT1 exhibited a better salt rejection of 97.4% as well as water permeance up to 11.9×10^4 GPU. The best overall desalination performance was observed when the PVA was crosslinked with MA and F-MWCNT, i.e., 99.9% of salt rejection with 7.4×10^4 GPU of water permeance. Likewise, the dehydration of ethanol was conducted as shown in Fig. 8b. The water content in the permeate side was 95.5 wt% (PVA-MA), 90.1 wt% (PVA-CNT1), 98.1 wt% (PVA-FCNT1) and 99.5 wt% (PVA-MA-FCNT1), resulting in separation factors of 505.3, 216.7, 1229.3 and 4738.1, respectively. The water permeance followed a similar trend as those in the desalination process yet with much lower values. It is reasonable that the permeance in the desalination process was higher than that of ethanol dehydration process because the aqueous salt solution as the feed contained many more free water molecules following a pseudo-liquid mixture mode. On the other hand, considering that the ethanol content in the feed was much higher than NaCl (96 wt% : 3.5 wt%), better separation performance was obtained during the ethanol dehydration process, implying an intrinsic difference between these two PV processes. For desalination, NaCl was unable to permeate through the membrane in its crystalloid state and thus the transport was realized by the hydration of the Na^+ and Cl^- ions and then the dissolution into the membrane. In order to keep charge neutrality, both hydrated Na^+ ions and Cl^- ions permeated through the membrane stoichiometrically. For separation of ethanol-water mixture, ethanol formed hydrogen bonding with water while kept its molecularity. PVA showed

a preferential adsorption selectivity for water as discussed in the swelling test.

For further investigation, the effect of feed concentration was investigated as illustrated in Fig. 9. Overall, the water permeance was positively correlated to the water content in the feed as a result of the sorption of water at the liquid/membrane interface. For PVA-MA, PVA-CNT1 and PVA-FCNT1, the salt rejections decreased when NaCl concentration in the feed grew gradually, while the ethanol in the permeate (otherwise the water content in the permeate) increased with water concentration in the feed. Therefore, it could be identified that the water content played different roles in affecting the separation process. For desalination, diffusion of NaCl in the membrane exhibited a concentration-dependant effect due to the increased dissolution of NaCl in the membrane. However, for ethanol dehydration, the increase in water content caused the swelling of the PVA and thus a plasticization effect, which enhanced segmental polymer chain mobility [63] and decreased the selectivity between water and ethanol. Notably, the PVA-MA-FCNT1 had a stable performance in both PV processes with nearly complete rejections, proving that the crosslinked PVA with good swelling resistance hindered the transport of salts and alcohol effectively while allowing effective permeation of water molecules. Such good performance of PVA-MA-FCNT1 was further proven by comparison with PVA-FCNT1 in a 30 h ethanol dehydration test, in which PVA-MA-FCNT1 exhibited stable performance whereas the separation efficiency of PVA-FCNT1 declined with time (Fig. S3 in Supporting Information).

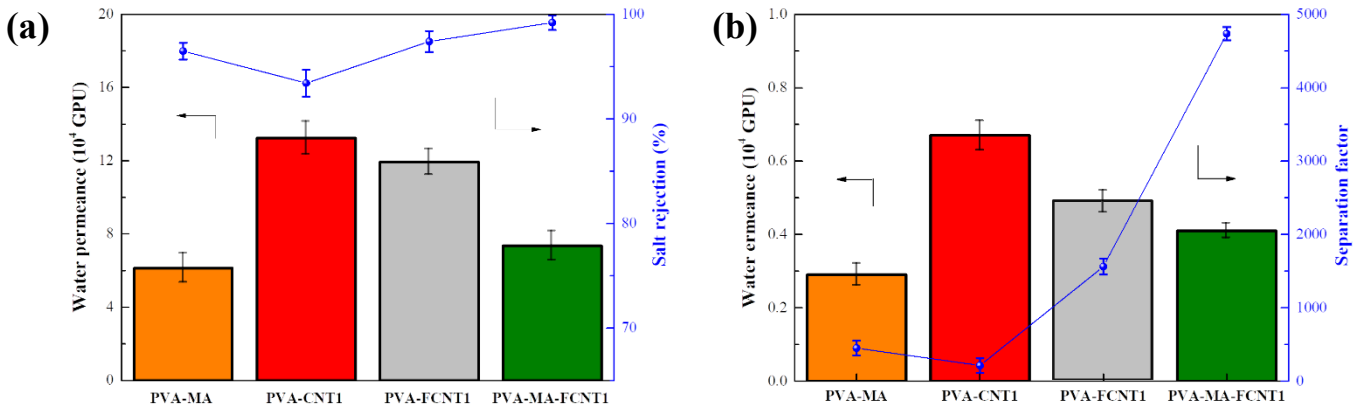

Fig. 8. PV performance of PVA-MA, PVA-CNT1, PVA-FCNT1 and PVA-MA-FCNT1 using (a) 3.5 wt% NaCl aqueous solution and (b) 96 wt% ethanol aqueous mixture at 30 °C.

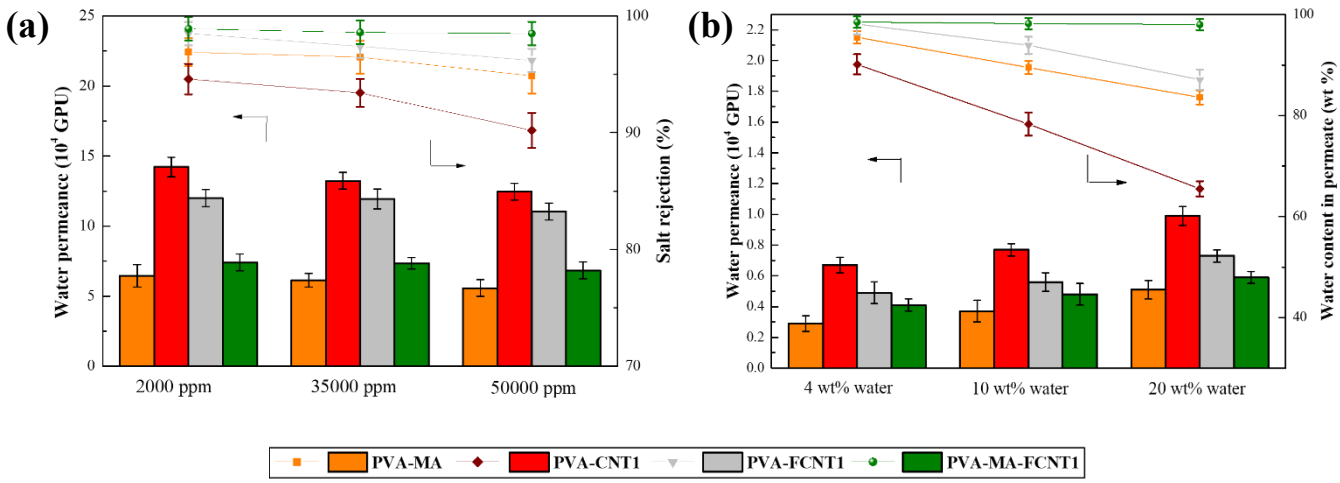

Fig. 9. PV performance under different feed concentrations at 30 °C.

The effect of feed temperature on the PV process was performed from 30 °C to 70 °C. The separation performance is displayed in Fig. 10, where gradual declines of water permeance with temperature were observed. This is mainly due to the rapid increase in the partial vapor pressure of water (31.84 Torr for 30 °C, 92.58 Torr for 50 °C and 233.84 Torr for 70 °C) in the feed side after normalizing the driving force. The temperature dependency of the transport can be analysed using an Arrhenius-type equation. Activation energy (E_a) for water, hydrated Na^+ ions (same with Cl^- ions) and

ethanol transport were listed in Table 4 (logarithmic plots using Eq 14 in Fig.S2 in Supporting Information). As discussed above, NaCl dissociated and water molecules formed concentric hydration shells around the ions. Ethanol was also dissolved by forming hydrogen bonds with water. From the PALS results in 3.2.3, the average pore sizes of the PVA based hybrid membranes were smaller than the hydrated sizes of ions and ethanol (0.66 nm for Cl^-, 0.72 nm for Na^+ and 0.68 nm for ethanol). Hence, permeation of salt through the free volume might be realized upon removing some water molecules from the hydration shell to form smaller hydrated ions or ethanol. The E_a demonstrated the energy barrier for permeation and the solutes with higher E_a were expected to experience larger energy barriers for entry into the free volume and exponentially smaller permeation rates. The activation energy for permeation of NaCl was higher than ethanol or water, indicating that NaCl required more energy to permeate through. In addition, as a volatile compound, ethanol has an increasing partial vapor pressure difference across the membrane when temperature is increased. That contributes to the enhanced ethanol transport through the membrane.

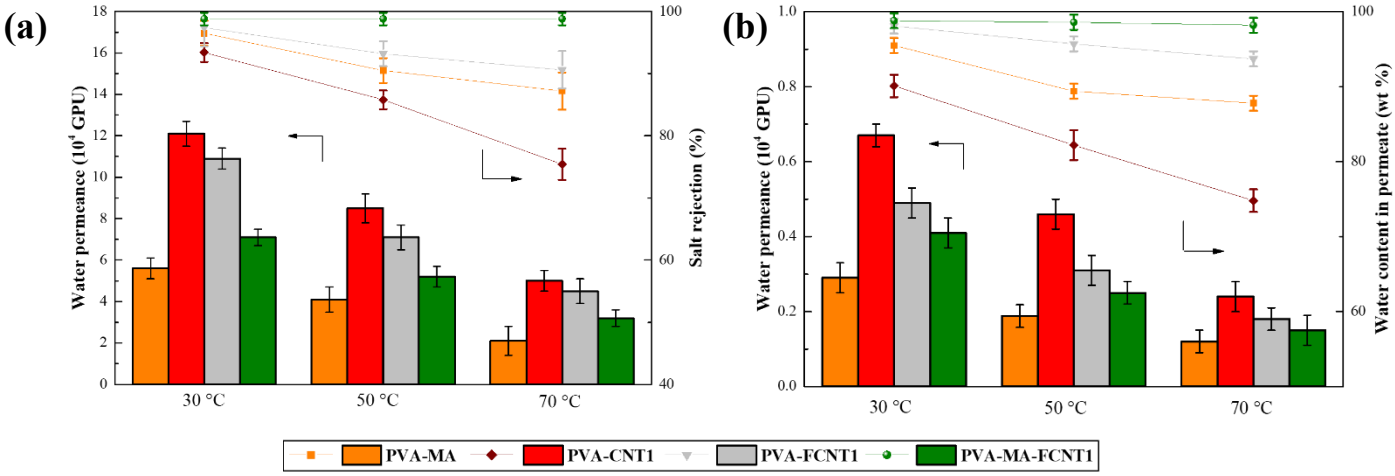

Fig. 10. PV performance vs. different feed temperatures; (a) desalination of 3.5 wt% NaCl solution; (b) dehydration of 96 wt% ethanol aqueous mixture.

Table 4

The activation energy for permeation of the PVA based hybrid membranes (kJ/mol).

Permeates	PVA-MA	PVA-CNT1	PVA-FCNT1	PVA-MA-FCNT1
water	21.70	21.20	22.19	24.19
ethanol	46.31	44.73	44.48	43.40
Na^+	49.47	49.80	49.88	49.30

3.3.2. Effects of CNT on water transport and separation

To further investigate the contribution of CNT to the water permeation mechanism of the PVA based hybrid membranes, water solubility and diffusivity were calculated. Fig. 11 shows the variation of solubility (dimensionless) and diffusivity (cm^2/s) before and after the addition of CNT scaled on that of PVA-MA (Q-t relation in Fig.S4 in the Supporting Information). As shown, PVA-CNT1 and PVA-FCNT1 had increased water solubilities while PVA-MA-FCNT1 showed a decreased one. Notably, the diffusivities were all elevated (85% for PVA-CNT1, 77% for PVA-FCNT1 and 56% for PVA-MA-FCNT1). As both the solubility and diffusivity contributed to the water transport through the membranes according to the solution-diffusion theory, the evolution implied that the water transport was altered to a diffusion-controlled type with reinforced interfacial interactions between CNT and PVA. It was demonstrated earlier that the incorporation of CNT increased the FFV (Fig. 7) and therefore favoured water transport. However, taking the PVA-FCNT1 for example, the increase in the FFV was only increasing 43% compared with the PVA-MA, while that of diffusivity is 77%. This may imply that the F-MWCNT contributed to the fast water transport synergistically as extra water transport channel. More specifically, the TEM image of PVA-FCNT1 is employed to illustrate transport with nanochannels as shown in Fig. 12. The F-MWCNT was distributed uniformly in the polymer. The proposed transport was that water permeated through the polymer matrix with dispersed

587 nanochannels. When they encountered F-MWCNT, the transport was enhanced by flowing through the
588 hollow space or along the outer surface. The overall water permeation was facilitated as the F-
589 MWCNT contributed to water transport partly along the whole water permeation path through the
590 membrane. It is worth mentioning that the dispersion state of CNT in the polymer plays an important
591 role in determining the separation performance. As MWCNT is hydrophobic, there is an strong
592 tendency to be immobilized in bundles, thus increasing the probability of defects. Finally, the effect of
593 CNT loading on the separation performance is shown in Fig.13. For the blended hybrid membranes
594 (PVA-CNT and PVA-FCNT), the water permeation increased with MWCNT and F-MWCNT (from
595 0.5 wt% to 2 wt%) as the number of nanochannels in the polymer matrix were rising. For PVA-MA-
596 FCNT, the water permeance decreased at 1% CNT loading, which implied that the transport was
597 hindered by increased crosslinking. While when the CNT loading reached 2%, the water permeance
598 was the highest for all the membranes. That might be the result of F-MWCNT agglomeration in the
599 membrane when the concentration of nanofiller was relatively high as shown in SEM (Fig.5).
600 Corresponding salt permeability and ethanol permeance were also depicted in Fig.14. The PVA-CNT
601 membranes had much higher salt permeabilities than PVA-FCNT and PVA-MA-FCNT membranes,
602 which can be attributed to their higher swelling. That negatively augmented the solubility of NaCl in
603 the membrane [32]. Further, the poor dispersion and lack of functional groups of CNT were conductive
604 to nonselective transport through the membrane [37]. Therefore, the high salt permeability proved
605 inferior for salt rejection of the PVA-CNT membranes. Similar trend was also observed for the ethanol
606 permeance. It should be noted that there were significant increases in both the salt and ethanol transport
607 at 2 wt% loading of MWCNT and F-MWCNT, implying the nonselective microscopic defects had
608 already existed in the membrane, elevating the nonselective transport in line with the above water

permeance results.

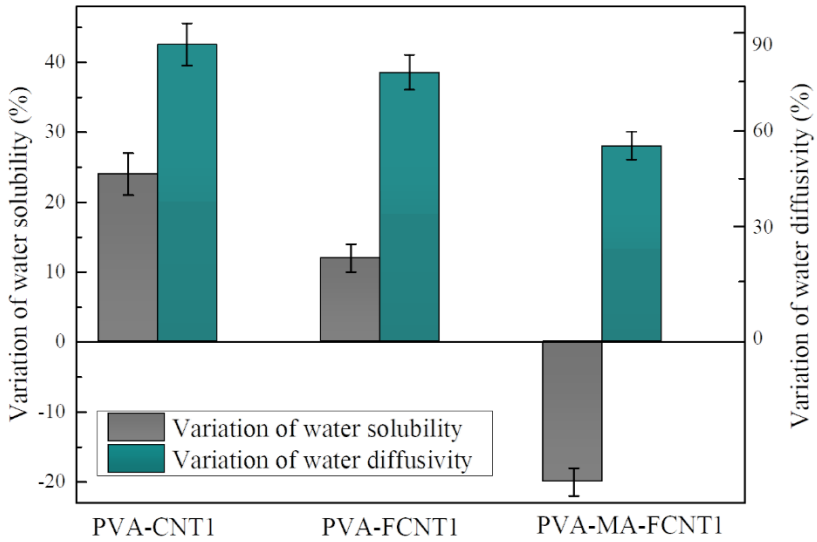

Fig. 11. Variations of water solubility and diffusivity compared with PVA-MA.

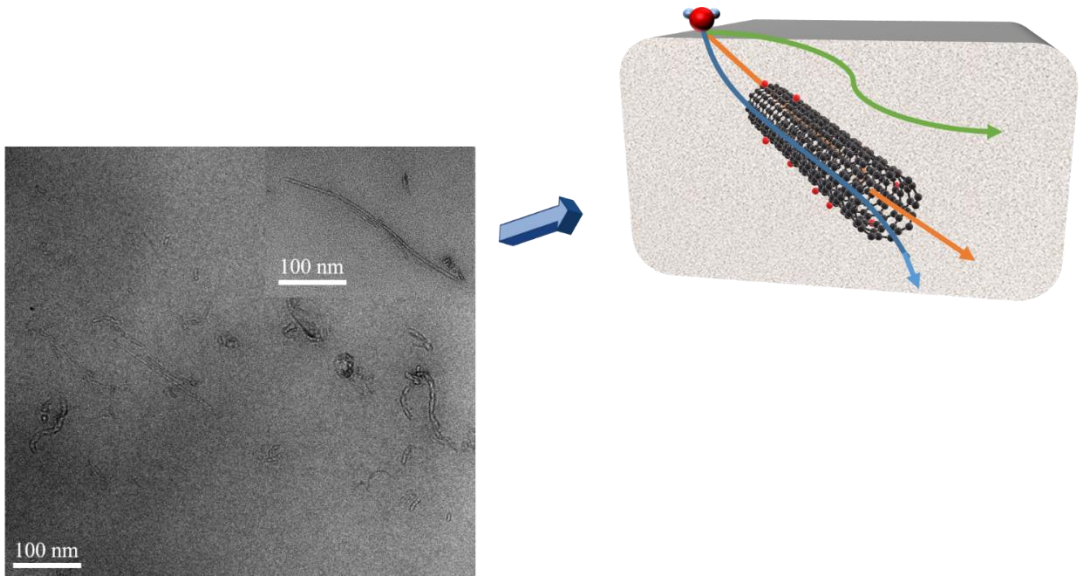

Fig. 12. TEM image of PVA-FCNT1 (enlarged CNT image inserted) with proposed water transport mechanism. The green transport path showed the permeation through polymer phase; The blue path represented a partially affected permeation path via polymer phase and outer surface of F-MWCNT; The orange path indicated a combined path of polymer phase and through-hollow-space of F-MWCNT.

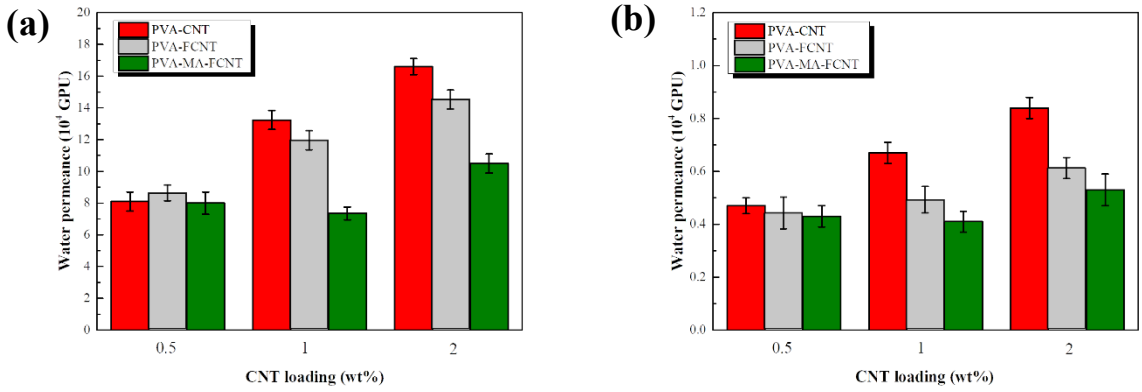

Fig. 13. Water permeance change with CNT loading; (a) water permeance in desalination by PV and (b) water permeance in dehydration of ethanol by PV.

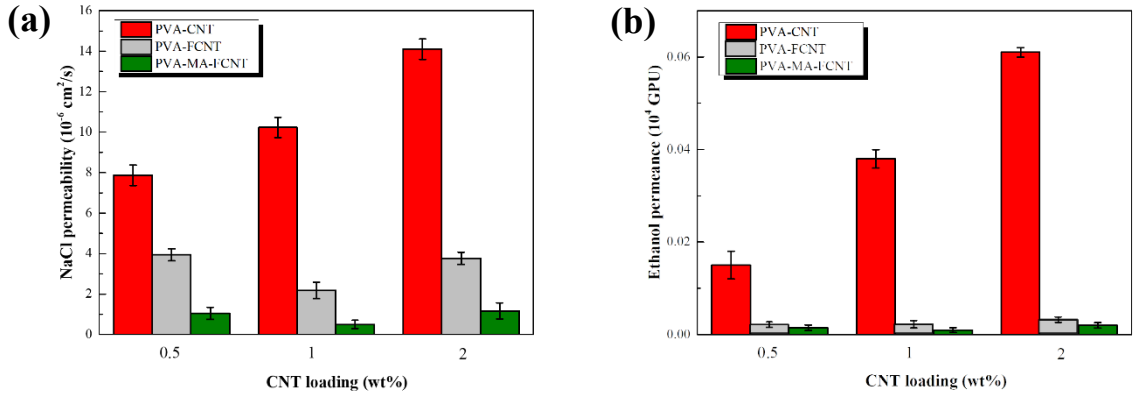

Fig. 14. Salt and ethanol transport with CNT loading; (a) NaCl permeability with CNT loading and (b) ethanol permeance with CNT loading.

4. Conclusions

In this work, PVA/CNT hybrid membranes with different combinations were employed to investigate the functions of the polymer and CNT in the PV separation processes of water/NaCl and water/ethanol. For the PVA matrix, the incorporation of CNT induced an increase in both the free volume cavity diameter and the fractional free volume, which is favourable for the water transport through the membranes. The states of the polymer in various solvents were found to be responsible for the separation of ions/water and ethanol/water. The PVA showed inherent adsorption affinity of water over ethanol, which significantly affected the polymer chain mobility and the crystalline structure.

Compared with the blended membranes (PVA-CNT1 and PVA-FCNT1), the PVA-MA-FCNT1 membrane was proven to have high separation performance with nearly complete rejection of ions and ethanol. The water diffusion results further implied enhanced water transport potentially brought by the CNT with additional fast water transport paths. Overall, this work provided a comprehensive study on how the polymer and nanofillers contributed to the separation of aqueous mixtures, benefiting the judicious design of polymer-based hybrid membranes and applications.

Supporting information

The comparison of FTIR spectra between PVA-FCNT and PVA-MA; Logarithmic plots of the Arrhenius relationship of the membranes; Long-term ethanol dehydration; Water contact angle results; Raw data of PALS and permeation fluxes; Summary of reported membrane performance compared with the PVA based membranes can be found in the supporting information.

Acknowledgments

The authors would like to acknowledge the financial support from Victoria University and CSIRO Manufacturing. Guang Yang gratefully acknowledges the scholarship from China Scholarship Council (CSC). Special thanks are given to Dr. Mark Greaves (CSIRO) and Dr. Malisja de Vries (CSIRO) for the FESEM training, Dr. Jacinta White (CSIRO) for TEM tests, and Dr. Aaron Seeber (CSIRO) for XRD tests, Dr Nouman Mirza (CSIRO) for permeance calculation and Mr Kewei Cai (CSIRO) for the experimental help in this work.

References

[1] X. Cheng, F. Pan, M. Wang, W. Li, Y. Song, G. Liu, H. Yang, B. Gao, H. Wu, Z. Jiang, Hybrid membranes for pervaporation separations, J. Membr. Sci., 541 (2017) 329-346.

[2] J.G. Wijmans, R.W. Baker, The solution-diffusion model: a review, J. Membr. Sci., 107 (1995) 1-21.

[3] Q. Wang, N. Li, B. Bolto, M. Hoang, Z. Xie, Desalination by pervaporation: A review, Desalination, 387 (2016) 46-60.

[4] Y. El Rayess, C. Albasi, P. Bacchin, P. Taillandier, J. Raynal, M. Mietton-Peuchot, A. Devatine, Cross-flow microfiltration applied to oenology: A review, J. Membr. Sci., 382 (2011) 1-19.

[5] C.-F. de Lannoy, E. Soyer, M.R. Wiesner, Optimizing carbon nanotube-reinforced polysulfone ultrafiltration membranes through carboxylic acid functionalization, J. Membr. Sci., 447 (2013) 395-402.

[6] A.W. Mohammad, Y.H. Teow, W.L. Ang, Y.T. Chung, D.L. Oatley-Radcliffe, N. Hilal, Nanofiltration membranes review: Recent advances and future prospects, Desalination, 356 (2015) 226-254.

[7] C. Fritzmann, J. Löwenberg, T. Wintgens, T. Melin, State-of-the-art of reverse osmosis desalination, Desalination, 216 (2007) 1-76.

[8] G. Liu, W. Wei, W. Jin, Pervaporation Membranes for Biobutanol Production, ACS Sustainable Chemistry & Engineering, 2 (2013) 546-560.

[9] P.D. Chapman, T. Oliveira, A.G. Livingston, K. Li, Membranes for the dehydration of solvents by pervaporation, J. Membr. Sci., 318 (2008) 5-37.

[10] A. Alkhudhiri, N. Darwish, N. Hilal, Membrane distillation: A comprehensive review, Desalination, 287 (2012) 2-18.

[11] G. Liu, Z. Jiang, C. Chen, L. Hou, B. Gao, H. Yang, H. Wu, F. Pan, P. Zhang, X. Cao, Preparation of ultrathin, robust membranes through reactive layer-by-layer (LbL) assembly for pervaporation dehydration, J. Membr. Sci., 537 (2017) 229-238.

[12] P. Shao, R.Y.M. Huang, Polymeric membrane pervaporation, J. Membr. Sci., 287 (2007) 162-179.

[13] B. Liang, W. Zhan, G. Qi, S. Lin, Q. Nan, Y. Liu, B. Cao, K. Pan, High performance graphene oxide/polyacrylonitrile composite pervaporation membranes for desalination applications, J. Mater. Chem. A, 3 (2015) 5140-5147.

[14] Z. Xie, M. Hoang, T. Duong, D. Ng, B. Dao, S. Gray, Sol–gel derived poly(vinyl alcohol)/maleic acid/silica hybrid membrane for desalination by pervaporation, J. Membr. Sci., 383 (2011) 96-103.

[15] Z.-l. Xu, L.-y. Yu, L.-f. Han, Polymer-nanoinorganic particles composite membranes: a brief overview, Frontiers of Chemical Engineering in China, 3 (2009) 318-329.

[16] R. Guo, X. Ma, C. Hu, Z. Jiang, Novel PVA–silica nanocomposite membrane for pervaporative dehydration of ethylene glycol aqueous solution, Polymer, 48 (2007) 2939-2945.

[17] J.J. Richardson, M. Bjornmalm, F. Caruso, Technology-driven layer-by-layer assembly of nanofilms, Science, 348 (2015) aaa2491.

[18] Z. Xie, D. Ng, M. Hoang, T. Duong, S. Gray, Separation of aqueous salt solution by pervaporation through hybrid organic–inorganic membrane: Effect of operating conditions, Desalination, 273 (2011) 220-225.

[19] S.Q. Dai, Y.Y. Jiang, T. Wang, L.G. Wu, X.Y. Yu, J.Z. Lin, S.X. Shi, Enhanced performance of polyimide hybrid membranes for benzene separation by incorporating three-dimensional silver-graphene oxide, J. Colloid Interface Sci., 478 (2016) 145-154.

[20] K. Cao, Z. Jiang, X. Zhang, Y. Zhang, J. Zhao, R. Xing, S. Yang, C. Gao, F. Pan, Highly water-selective hybrid membrane by incorporating g-C3N4 nanosheets into polymer matrix, J. Membr. Sci., 490 (2015) 72-83.

[21] B. Gao, Z. Jiang, G. Liu, R. Xing, H. Wu, F. Pan, B. Wang, X. Cao, Enhanced pervaporative performance of hybrid membrane by incorporating amphiphilic carbonaceous material, J. Membr. Sci., 520 (2016) 951-963.

[22] Y.K. Ong, G.M. Shi, N.L. Le, Y.P. Tang, J. Zuo, S.P. Nunes, T.-S. Chung, Recent membrane development for pervaporation

processes, Prog. Polym. Sci., 57 (2016) 1-31.
[23] M.E. Dmitrenko, A.V. Penkova, A.B. Missyul, A.I. Kuzminova, D.A. Markelov, S.S. Ermakov, D. Roizard, Development and investigation of mixed-matrix PVA-fullerenol membranes for acetic acid dehydration by pervaporation, Sep. Purif. Technol., 187 (2017) 285-293.
[24] Y. Shirazi, T. Mohammadi, Effects of CNTs Content on Physicochemical and Pervaporation Separation Properties of PVA Membranes, Sep. Sci. Technol., 48 (2013) 716-727.
[25] B. Bolto, T. Tran, M. Hoang, Z. Xie, Crosslinked poly(vinyl alcohol) membranes, Prog. Polym. Sci., 34 (2009) 969-981.
[26] L.L. Xia, C.L. Li, Y. Wang, In-situ crosslinked PVA/organosilica hybrid membranes for pervaporation separations, J. Membr. Sci., 498 (2016) 263-275.
[27] S. Khoonsap, S. Rugmai, W.-S. Hung, K.-R. Lee, S. Klinsrisuk, S. Amnuaypanich, Promoting permeability-selectivity anti-trade-off behavior in polyvinyl alcohol (PVA) nanocomposite membranes, J. Membr. Sci., 544 (2017) 287-296.
[28] Z. Huang, Y. Shi, R. Wen, Y. Guo, J. Su, T. Matsuura, Multilayer poly(vinyl alcohol)–zeolite 4A composite membranes for ethanol dehydration by means of pervaporation, Sep. Purif. Technol., 51 (2006) 126-136.
[29] Z. Xie, M. Hoang, D. Ng, C. Doherty, A. Hill, S. Gray, Effect of heat treatment on pervaporation separation of aqueous salt solution using hybrid PVA/MA/TEOS membrane, Sep. Purif. Technol., 127 (2014) 10-17.
[30] M. Sairam, M. Patil, R. Veerapur, S. Patil, T. Aminabhavi, Novel dense poly(vinyl alcohol)–TiO2 mixed matrix membranes for pervaporation separation of water – isopropanol mixtures at 30° C☆, J. Membr. Sci., 281 (2006) 95-102.
[31] Z. Jia, G. Wu, Metal-organic frameworks based mixed matrix membranes for pervaporation, Microporous Mesoporous Mater., 235 (2016) 151-159.
[32] G. Yang, Z. Xie, M. Cran, D. Ng, S. Gray, Enhanced desalination performance of poly (vinyl alcohol)/carbon nanotube composite pervaporation membranes via interfacial engineering, J. Membr. Sci., 579 (2019) 40-51.
[33] R.L.G. Lecaros, K.M. Deseo, W.-S. Hung, L.L. Tayo, C.-C. Hu, Q.-F. An, H.-A. Tsai, K.-R. Lee, J.-Y. Lai, Influence of integrating graphene oxide quantum dots on the fine structure characterization and alcohol dehydration performance of pervaporation composite membrane, J. Membr. Sci., 576 (2019) 36-47.
[34] B. Gao, Z. Jiang, C. Zhao, H. Gomaa, F. Pan, Enhanced pervaporative performance of hybrid membranes containing Fe3O4@CNT nanofillers, J. Membr. Sci., 492 (2015) 230-241.
[35] H.-D. Huang, P.-G. Ren, J. Chen, W.-Q. Zhang, X. Ji, Z.-M. Li, High barrier graphene oxide nanosheet/poly(vinyl alcohol) nanocomposite films, J. Membr. Sci., 409-410 (2012) 156-163.
[36] C. Xue, G.Q. Du, L.J. Chen, J.G. Ren, J.X. Sun, F.W. Bai, S.T. Yang, A carbon nanotube filled polydimethylsiloxane hybrid membrane for enhanced butanol recovery, Sci Rep, 4 (2014) 5925.
[37] H.J. Kim, K. Choi, Y. Baek, D.G. Kim, J. Shim, J. Yoon, J.C. Lee, High-performance reverse osmosis CNT/polyamide nanocomposite membrane by controlled interfacial interactions, ACS Appl Mater Interfaces, 6 (2014) 2819-2829.
[38] Ihsanullah, Carbon nanotube membranes for water purification: Developments, challenges, and prospects for the future, Sep. Purif. Technol., 209 (2019) 307-337.
[39] S. Li, G. Liao, Z. Liu, Y. Pan, Q. Wu, Y. Weng, X. Zhang, Z. Yang, O.K.C. Tsui, Enhanced water flux in vertically aligned carbon nanotube arrays and polyethersulfone composite membranes, J. Mater. Chem. A, 2 (2014) 12171-12176.
[40] K. Gethard, O. Sae-Khow, S. Mitra, Water desalination using carbon-nanotube-enhanced membrane distillation, ACS Appl Mater Interfaces, 3 (2011) 110-114.
[41] B. Corry, Water and ion transport through functionalised carbon nanotubes: implications for desalination technology, Energy & Environmental Science, 4 (2011) 751.
[42] J.-H. Choi, J. Jegal, W.-N. Kim, H.-S. Choi, Incorporation of multiwalled carbon nanotubes into poly(vinyl alcohol) membranes for use in the pervaporation of water/ethanol mixtures, J. Appl. Polym. Sci., 111 (2009) 2186-2193.
[43] Y. Shirazi, M.A. Tofighy, T. Mohammadi, Synthesis and characterization of carbon nanotubes/poly vinyl alcohol nanocomposite membranes for dehydration of isopropanol, J. Membr. Sci., 378 (2011) 551-561.

[44] F. Peng, C. Hu, Z. Jiang, Novel ploy(vinyl alcohol)/carbon nanotube hybrid membranes for pervaporation separation of benzene/cyclohexane mixtures, J. Membr. Sci., 297 (2007) 236-242.
[45] M. Elkashef, K. Wang, M.N. Abou-Zeid, Acid-treated carbon nanotubes and their effects on mortar strength, Frontiers of Structural and Civil Engineering, 10 (2015) 180-188.
[46] S. Sahebian, S.M. Zebarjad, J. vahdati Khaki, A. Lazzeri, A study on the dependence of structure of multi-walled carbon nanotubes on acid treatment, Journal of Nanostructure in Chemistry, 5 (2015) 287-293.
[47] Q.G. Zhang, Q.L. Liu, Y. Chen, J.Y. Wu, A.M. Zhu, Microstructure dependent diffusion of water–ethanol in swollen poly(vinyl alcohol): A molecular dynamics simulation study, Chem. Eng. Sci., 64 (2009) 334-340.
[48] J. Kamcev, C.M. Doherty, K.P. Lopez, A.J. Hill, D.R. Paul, B.D. Freeman, Effect of fixed charge group concentration on salt permeability and diffusion coefficients in ion exchange membranes, J. Membr. Sci., 566 (2018) 307-316.
[49] J. Kansy, Microcomputer program for analysis of positron annihilation lifetime spectra Nuclear Instmments and Methods in Physics Research A 374 (1996) 235-244.
[50] G.M. Geise, C.M. Doherty, A.J. Hill, B.D. Freeman, D.R. Paul, Free volume characterization of sulfonated styrenic pentablock copolymers using positron annihilation lifetime spectroscopy, J. Membr. Sci., 453 (2014) 425-434.
[51] B. Liang, Q. Li, B. Cao, P. Li, Water permeance, permeability and desalination properties of the sulfonic acid functionalized composite pervaporation membranes, Desalination, 433 (2018) 132-140.
[52] F. Peng, F. Pan, H. Sun, L. Lu, Z. Jiang, Novel nanocomposite pervaporation membranes composed of poly(vinyl alcohol) and chitosan-wrapped carbon nanotube, J. Membr. Sci., 300 (2007) 13-19.
[53] G. Dudek, P. Borys, A Simple Methodology to Estimate the Diffusion Coefficient in Pervaporation-Based Purification Experiments, Polymers (Basel), 11 (2019).
[54] H. Ju, A.C. Sagle, B.D. Freeman, J.I. Mardel, A.J. Hill, Characterization of sodium chloride and water transport in crosslinked poly(ethylene oxide) hydrogels, J. Membr. Sci., 358 (2010) 131-141.
[55] K. Huang, G. Liu, Y. Lou, Z. Dong, J. Shen, W. Jin, A graphene oxide membrane with highly selective molecular separation of aqueous organic solution, Angew. Chem. Int. Ed. Engl., 53 (2014) 6929-6932.
[56] S. Panahian, A. Raisi, A. Aroujalian, Multilayer mixed matrix membranes containing modified-MWCNTs for dehydration of alcohol by pervaporation process, Desalination, 355 (2015) 45-55.
[57] M.Z. Rong, M.Q. Zhang, W.H. Ruan, Surface modification of nanoscale fillers for improving properties of polymer nanocomposites: a review, Mater. Sci. Technol., 22 (2013) 787-796.
[58] P. Akcora, H. Liu, S.K. Kumar, J. Moll, Y. Li, B.C. Benicewicz, L.S. Schadler, D. Acehan, A.Z. Panagiotopoulos, V. Pryamitsyn, V. Ganesan, J. Ilavsky, P. Thiyagarajan, R.H. Colby, J.F. Douglas, Anisotropic self-assembly of spherical polymer-grafted nanoparticles, Nat Mater, 8 (2009) 354-359.
[59] H.S. Mansur, M.M. Pereira, H.S. Costa, A.A.P. Mansur, Mechanical Behavior of Nanostructured Hybrids Based on Poly(Vinyl Alcohol)/Bioactive Glass Reinforced with Functionalized Carbon Nanotubes, Journal of Nanomaterials, 2012 (2012) 1-9.
[60] R. Ricciardi, F. Auriemma, C.D. Rosa, F. Laupretre, X-ray Diffraction Analysis of Poly(vinyl alcohol) Hydrogels, Obtained by Freezing and Thawing Techniques, Macromolecules 37, (2004) 1921-1927.
[61] R. Wang, Q. Wang, L. Li, Evaporation behaviour of water and its plasticizing effect in modified poly(vinyl alcohol) systems, Polym. Int., 52 (2003) 1820-1826.
[62] G. Choudalakis, A.D. Gotsis, Free volume and mass transport in polymer nanocomposites, Current Opinion in Colloid & Interface Science, 17 (2012) 132-140.
[63] M. Zhang, L. Deng, D. Xiang, B. Cao, S. Hosseini, P. Li, Approaches to Suppress CO2-Induced Plasticization of Polyimide Membranes in Gas Separation Applications, Processes, 7 (2019) 51-82.